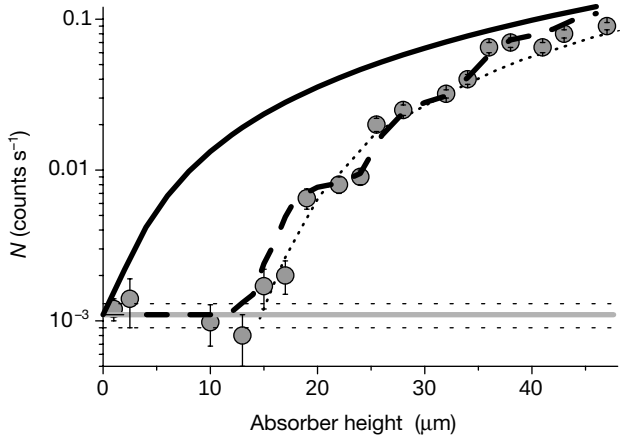

Figure 4 The neutron throughput versus the absorber height at low height values. The data points are summed up in intervals of 2 μm. The dashed curve corresponds to a fit using the quantum-mechanical calculation, in which all level populations and the height resolution are fitted from the experimental data. The solid curve is again the full classical treatment. The dotted line is a truncated fit in which it is assumed that only the lowest quantum state—which leads to the first step—exists.

curve shows the results of a quantum fit, in which the level populations and the height resolution are free parameters. The solid line is again the full classical treatment ($N \sim z^{1.5}$). The dotted line is a truncated fit to the assumption that only the lowest quantum level—which leads to the first step—exists. Then it continues at the absorber height of $z_1 \approx 15\,\mu m$ with a shifted classical treatment ($N \sim (z - z_1)^{1.5}$) that is more like a 'guide to the eye' curve. Our statistics for large slit width are still not sufficient, but the existence of the first step due to the lowest quantum level is clearly reproduced.

Our experimental observations of the neutron quantum states in the Earth's gravitational field provide another demonstration of the universality of the quantum properties of matter, but at this stage we have only shown a phenomenon that was expected—although not easy to prove. As the parameters of quantum states are defined in such a system mainly by the interaction of the neutron with the gravitational field, the phenomenon we report can now be considered for further investigations of fundamental properties of matter. Thus, as it is evident from the uncertainty principle, the energy resolution ΔE could be improved significantly by increasing $\Delta\tau$ (in principle, ΔE could be as low as $\sim 10^{-18}$ eV if $\Delta\tau$ approaches the lifetime of the neutron, so that the level width becomes a million times smaller than the energy difference between levels). The use of resonance transitions between such narrow levels could find applications in physics, such as the precise verification of the proportionality of inertial and gravitational masses of elementary particles (neutrons), and a check of the electrical neutrality of neutrons—which is not a trivial fact. Increasing the time that neutrons spend in the gravitational bound states will become one of the main challenges in extending this experiment. When trying to achieve this, it will be necessary to demonstrate that the neutrons are spending a much longer time in the potential well, and a significant increase in the available density of ultracold neutrons will be necessary. □

Received 10 October; accepted 22 November 2001.

1. Luschikov, V. I. & Frank, A. I. Quantum effects occurring when ultracold neutrons are stored on a plane. *JETP Lett.* **28,** 559–561 (1978).
2. Nesvizhevsky, V. V. *et al.* Search for quantum states of the neutron in a gravitational field: gravitational levels. *Nucl. Instrum. Methods Phys. Res.* **440,** 754–759 (2000).
3. Nesvizhevsky, V. V. *et al.* in *ILL Annual Report* (eds Cicognani, G. & Vettier, Ch.) 64–65 (Institute Laue-Langevin, Grenoble, 2000).
4. Landau, L. D. & Lifshitz, E. M. *Quantum Mechanics* 164–196 (Pergamon, Oxford, 1976).
5. Flügge, S. *Practical Quantum Mechanics* (Mir, Moscow, 1974).
6. Colella, R. A., Overhauser, W. & Werner, W. A. Observation of gravitationally induced quantum interference. *Phys. Rev. Lett.* **34,** 1472–1474 (1975).
7. Baryshevskii, V. G., Chrerepitza, S. V. & Frank, A. I. Neutron spin interferometry. *Phys. Lett. A* **153,** 299–302 (1991).
8. Frank, A. I. Modern optics of long-wavelength neutrons. *Sov. Phys. Usp.* **34,** 980–987 (1991).
9. Felber, J., Gähler, R., Rauch, C. & Golub, R. Matter waves at a vibrating surface: Transition from quantum-mechanical to classical behavior. *Phys. Rev. A* **53,** 319–328 (1996).
10. Peters, A., Chung, K. Y. & Chu, S. Measurement of gravitational acceleration by dropping atoms. *Nature* **400,** 849–852 (1999).
11. Luschikov, V. I., Pokotilovsky, Yu. N., Strelkov, A. V. & Shapiro, F. L. Observation of ultracold neutrons. *JETP Lett.* **9,** 23–26 (1969).
12. Steyerl, A. Measurement of total cross sections for very slow neutrons with velocities from 100m/s to 5m/s. *Phys. Lett. B* **29,** 33–35 (1969).
13. Ignatovich, V. K. *The Physics of Ultracold Neutrons* (Clarendon, Oxford, 1990).
14. Golub, R., Richardson, D. J. & Lamoreux, S. K. *Ultracold Neutrons* (Higler, Bristol, 1991).
15. Steyerl, A. & Malik, S. S. Sources of ultracold neutrons. *Nucl. Instrum. Methods Phys. Res. A* **284,** 200–207 (1989).
16. Born, M. *Atomic Physics* (Blackie & Son, London, 1969).
17. Bohr, A. & Mottelson, B. R. *Nuclear Structure* (Benjamin, New York, 1969).

Acknowledgements

We are grateful to our colleagues who were interested in this research and contributed to its development, in particular K. Ben-Saidane, D. Berruyer, Th. Brenner, J. Butterworth, D. Dubbers, P. Geltenbort, T. M. Kuzmina, A. J. Leadbetter, B. G. Peskov, S. V. Pinaev, K. Protasov, I. A. Snigireva, S. M. Soloviev and A. Voronin. The work was supported by INTAS.

Competing interests statement

The authors declare that they have no competing financial interests.

Correspondence and requests for materials should be addressed to V.V.N. (e-mail: nesvizhevsky@ill.fr).

Antiferromagnetic order induced by an applied magnetic field in a high-temperature superconductor

B. Lake*†, H. M. Rønnow‡, N. B. Christensen§‖, G. Aeppli§¶, K. Lefmann§, D. F. McMorrow§, P. Vorderwisch#, P. Smeibidl#, N. Mangkorntong☆, T. Sasagawa☆, M. Nohara☆, H. Takagi☆ & T. E. Mason**

** Oak Ridge National Laboratory, PO Box 2008 MS 6430, Oak Ridge, Tennessee 37831-6430, USA*
† Department of Condensed Matter Physics, University of Oxford, Clarendon Laboratory Parks Road, Oxford OX1 3PU, UK
‡ CEA (MDN/SPSMS/DRFMC), 17 Ave. des Martyrs, 38054 Grenoble cedex 9, France
§ Materials Research Department, Risø National Laboratory, 4000 Roskilde, Denmark
‖ Ørsted Laboratory, Niels Bohr Institute for APG, Universitetsparken 5, DK 2100, Copenhagen, Denmark
¶ NEC Research Institute, 4 Independence Way, Princeton, New Jersey 08540-6634, USA
 # BENSC, Hahn-Meitner Institut, Glienicker Strasse 100, 14109 Berlin, Germany
☆ Department of Advanced Materials Science, Graduate School of Frontier Sciences, University of Tokyo, Hongo 7-3-1, Bunkyo-ku, Tokyo 113-8656, Japan
*** Experimental Facilities Division, Spallation Neutron Source, 701 Scarboro Road, Oak Ridge, Tennessee 37830, USA*

One view of the high-transition-temperature (high-T_c) copper oxide superconductors is that they are conventional superconductors where the pairing occurs between weakly interacting quasiparticles (corresponding to the electrons in ordinary metals), although the theory has to be pushed to its limit[1]. An alternative view is that the electrons organize into collective textures (for example, charge and spin stripes) which cannot be 'mapped' onto the electrons in ordinary metals. Understanding the properties of the material would then need quantum field theories of objects

such as textures and strings, rather than point-like electrons[2–6]. In an external magnetic field, magnetic flux penetrates type II superconductors via vortices, each carrying one flux quantum[7]. The vortices form lattices of resistive material embedded in the non-resistive superconductor, and can reveal the nature of the ground state—for example, a conventional metal or an ordered, striped phase—which would have appeared had superconductivity not intervened, and which provides the best starting point for a pairing theory. Here we report that for one high-T_c superconductor, the applied field that imposes the vortex lattice also induces 'striped' antiferromagnetic order. Ordinary quasiparticle models can account for neither the strength of the order nor the nearly field-independent antiferromagnetic transition temperature observed in our measurements.

$La_{2-x}Sr_xCuO_4$ is the simplest high-T_c superconductor. The undoped compound is an insulating antiferromagnet, where the spin moments on adjacent Cu^{2+} ions are antiparallel[8]. Introduction of charge carriers via Sr doping reduces the ordered moment until it vanishes at $x < 0.13$. In addition, for $x > 0.05$ the commensurate antiferromagnetism is replaced by incommensurate order[2,3,9,10], where the repeat distance for the pattern of ordered moments is substantially larger than the spacing between neighbouring copper ions. $La_{2-x}Sr_xCuO_4$ becomes a superconductor for Sr dopings of $0.06 < x < 0.25$, and for underdoped compounds ($0.06 < x < 0.13$), both superconductivity and magnetic order are present. Figure 1a shows the electrical resistivity as a function of temperature T and magnetic field H, applied perpendicularly to the superconducting CuO_2 planes, for a sample with $x = 0.10$. The resistivity decreases rapidly below the zero-field transition temperature $T_c(H = 0\,T) = 29\,K$, and becomes zero below the irreversibility temperature $T_{irr}(H)$. The white circles locate T_{irr} and show that it is a rapid function of applied field, so that even for fields much smaller than the upper critical field ($H_{c2}(x = 0.10) \approx 45\,T$; ref. 11), perfect conductivity does not occur until the temperature is well below $T_c(H = 0\,T)$.

In our experiments we used magnetic neutron diffraction to measure the spin ordering in single crystals of underdoped $La_{2-x}Sr_xCuO_4$ ($x = 0.10$). The technique is analogous to mapping the positions of atoms in crystals using X-ray or neutron diffraction. The superconducting CuO_2 planes were aligned in the scattering plane, and the magnetic field was applied perpendicular to these planes. The inset in Fig. 2a shows the reciprocal space region over which data were collected. In zero field (Fig. 2a), incommensurate elastic peaks occur in the superconducting phase at low-temperatures. The peaks are resolution-limited, implying an in-plane correlation length of $\zeta > 400$ Å, similar to that observed[10] for

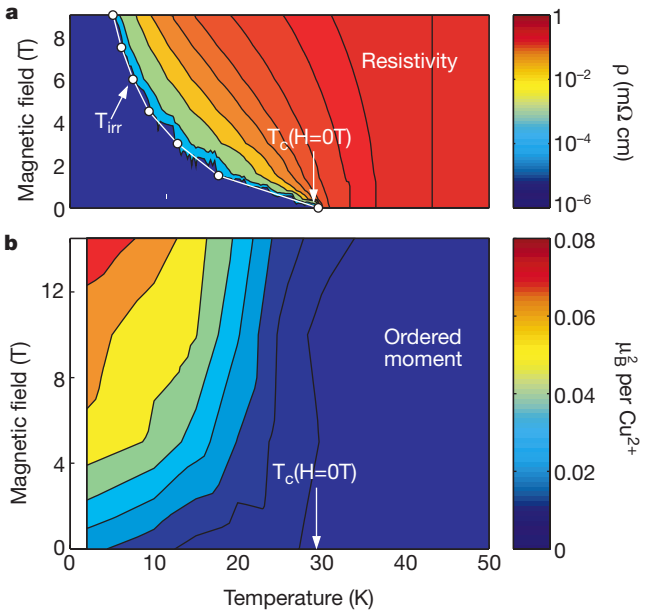

Figure 1 Magneto-transport and neutron diffraction data for $La_{2-x}Sr_xCuO_4$ as a function of temperature and magnetic field. **a**, Magneto-transport measurements parallel to the CuO_2 planes, obtained via a standard four-probe method; the colours indicate the electrical resistivity ρ. In a magnetic field, the sharp transition from normal to superconducting states is broadened into a crossover region and vortices are thought to form at temperatures where the resistivity falls below its value at $T_c(H = 0\,T)$. Phase coherent superconductivity, characterized by zero-resistivity sets in at the much lower 'irreversibility' temperature ($T_{irr}(H)$), marked by the white circles. **b**, The square of the ordered spin moment per Cu^{2+} ion as a function of temperature and applied magnetic field. The ordered moment squared is proportional to the observed neutron-scattering signal, and was deduced from scans similar to those shown in Fig. 2. It first becomes significant below the zero-field superconducting transition temperature ($T_c(H = 0\,T)$), and increases with decreasing temperature and increasing field. The crystals used for these measurements were grown in an optical image furnace.

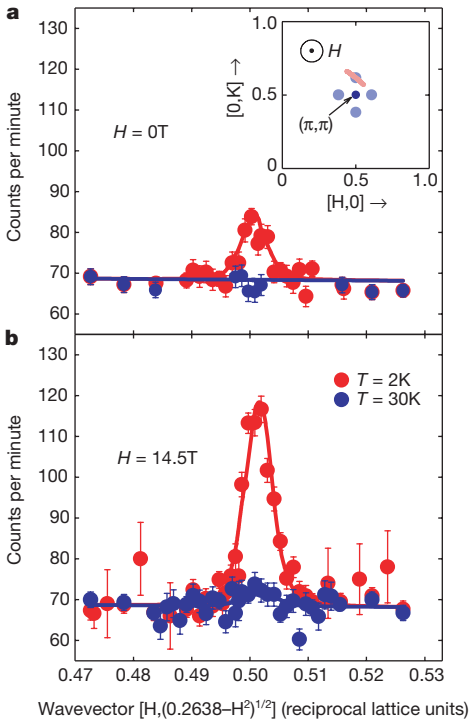

Figure 2 Magnetic neutron diffraction data for $La_{2-x}Sr_xCuO_4$ with $x = 0.10$. The inset shows the relevant reciprocal space, labelled using the two-dimensional notation appropriate for the superconducting CuO_2 planes. The black dot at (0.5,0.5) represents the Bragg point associated with the commensurate antiferromagnetism of the insulating $x = 0$ parent compound. The incommensurate antiferromagnetic order in our metallic $x = 0.10$ material gives rise to diffraction at the quartet of blue dots[10]. The pink line shows the trajectory of a typical scan which passes through the incommensurate peak at (0.5,0.6175) and the direction of the applied field is shown to be perpendicular to the CuO_2 planes. **a**, The data collected in zero field. The red circles show that signal is present in the superconducting phase at $T = 1.9$ K. But just above the superconducting transition temperature at $T = 30$ K, the signal has completely disappeared (blue circles). **b**, Data measured at the same temperatures as **a**, but in a field of $H = 14.5$ T; the low-temperature signal is a factor of three larger than the zero-field signal. The data were collected using the V2/FLEX neutron scattering spectrometer at the BER II reactor, Hahn-Meitner Institute, Berlin. 60′ collimators were used to define the divergence of the neutron beam. The energy was fixed at 7.5 meV using a pyrolytic graphite (PG) monochromator and analyser, and a tunable PG filter was used to eliminate second-order scattering.

$x = 0.12$. The peak amplitude decreases as T is increased, and is entirely absent at $T = 30$ K. Our new finding is that external magnetic fields markedly increase the low-temperature signal. Figure 2b shows that for $H = 14.5$ T and $T = 2$ K the signal is three times larger than in zero field, while at 30 K, just above $T_c(H = 0\,\mathrm{T})$, there is very little field-induced signal. The field-induced signal is resolution-limited, and the magnetic in-plane correlation length ($\zeta > 400$ Å), is much greater than the superconducting coherence length ($\xi \approx 20$ Å) and the inter-vortex spacing ($a_v = 130$ Å for $H = 14.5$ T). As the superconducting coherence length gives the size of the vortices, coherent magnetism cannot reside in the vortex cores alone, but must extend across the superconducting regions of the material. This result is important because, taken together with the strong antiferromagnetic proximity effect which follows from the large zero-frequency antiferromagnetic susceptibility of superconducting $La_{2-x}Sr_xCuO_4$ (ref. 12), it implies that as long as the vortex array is not radically different from a conventional Abrikosov lattice, superconductivity and antiferromagnetism coexist throughout the bulk of the material.

We collected scans similar to those shown in Fig. 2 for a variety of fields and temperatures. The neutron signal is normalized using a standard phonon-based calibration to yield the ordered spin moment squared, as displayed in Fig. 1b. Order develops just below the zero-field transition temperature $T_c(H = 0\,\mathrm{T})$, and increases with decreasing temperature and increasing field. Figure 3a shows the temperature dependence; the zero-field order (blue circles) increases gradually below $T_c(H = 0\,\mathrm{T})$, reaching a maximum of $0.15 \pm 0.01\,\mu_B$ per Cu^{2+} ion (μ_B is the Bohr magneton and the error is statistical). This value is somewhat larger than the value of $0.10 \pm 0.04\,\mu_B$ per Cu^{2+} deduced from neutron-diffraction measurements for a sample with $x = 0.12$ (ref. 13). The field-induced order for $H = 5$ T, 10 T and 14.5 T is also plotted; it was obtained by subtracting the zero-field signal from the signal measured in-field. The temperature dependence of the field-induced signal is clearly different from that for $H = 0$ T. It increases more rapidly just below $T_c(H = 0\,\mathrm{T})$ and saturates for $T < 10$ K, where in zero field the moment is still evolving. Figure 3b shows the H dependence of the field-induced order at base temperature ($T = 1.9$ K). The order increases rapidly with small fields, probably reflecting the linear dependence of vortex density on field. The order increases more slowly for higher fields as the antiferromagnetic regions, nucleated by the vortices, start to merge.

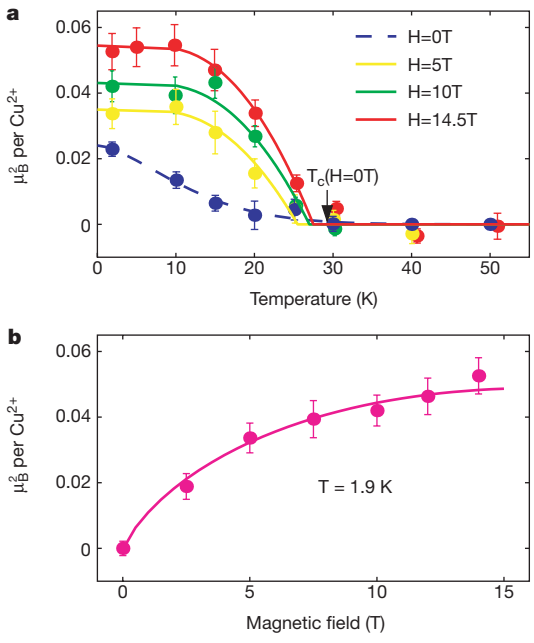

Figure 3 The dependence on temperature and field of the ordered spin moment squared. The data were calibrated using a transverse acoustic phonon measured around the (1,1) Bragg peak (energy transfer $E = 2$ meV and sound velocity = 26.9 meV Å), and are presented in units of μ_B^2 per Cu^{2+}. **a**, The temperature dependence. The zero-field signal (blue circles) increases gradually below $T_c(H = 0\,\mathrm{T})$, and the dashed line is a guide to the eye. Also plotted is the field-induced signal (equal to the signal measured in-field minus the zero-field signal) for fields of $H = 5$ T (yellow circles), 10 T (green circles) and 14.5 T (red circles). The solid lines through the data are fits to mean field theory[26]. **b**, The field-induced signal as a function of field at $T = 2$ K (magenta circles). The solid line is a fit to the data of the expression, $M^2(H/H_{c2})\ln(H_{c2}/H)$ (ref. 23), with fitted parameter $M^2 = 0.12\,\mu_B^2$ per Cu^{2+}.

Our work represents a departure from two previous experiments[14,15] on $La_{2-x}Sr_xCuO_4$ in magnetic fields. In the first experiment, the static magnetism in a sample with $x = 0.12$ was found to undergo an enhancement in an applied magnetic field consistent with our findings[14]. But this measurement was confined to a single field (10 T) and temperature (4.2 K), and the sample was atypical—with an anomalously low value of $T_c(H = 0\,\mathrm{T}) = 12$ K. The zero-field Néel temperature, $T_N = 25$ K, was well above $T_c(H = 0\,\mathrm{T})$, and the onset temperature for the field-induced enhancement was unknown. The second experiment focused on magnetic dynamics in optimally doped $La_{2-x}Sr_xCuO_4$ ($x = 0.163$) (ref. 15). This material showed no static magnetism in either zero or non-zero fields up to 14.5 T. But an applied field had the effect of recovering some of the magnetic fluctuations below the 'spin gap' which are suppressed by superconductivity in zero field. An important feature of this experiment was that the antiferromagnetic correlations developed at a temperature below T_{irr}; that is, they only occurred once phase coherent superconductivity had been attained. Thus the results of ref. 15 are in some ways the inverse or 'dual' of those we report here on our sample with $x = 0.1$, where the static antiferromagnetism arises first and phase coherent superconductivity is established at a lower temperature, when the ordered moments have saturated near their base temperature values.

We believe that the field-induced signal is intrinsic, and arises from fundamental physical processes, even though the zero-field signal may well be stabilized by the disorder inherent in a random alloy such as $La_{2-x}Sr_xCuO_4$. Thus, the magnetic field does not simply enhance the existing antiferromagnetism but induces magnetic order in its own right. There are several reasons to support our belief. First, the sample is of very high quality, as shown by specific heat measurements[16] and our transport data (Fig. 1a). Second, a different and poorer-quality sample, also with $x = 0.10$, which displays static antiferromagnetism in zero field above as well as below $T_c(H = 0\,\mathrm{T})$, showed field-induced order with exactly the same temperature dependence as reported here[17]. Third, the degree of order is substantial, corresponding to a volume fraction of ~50% for the incommensurate magnetic state, assuming that the ordered moment is $0.4\mu_B$ per Cu^{2+}, as suggested by muon spin relaxation data[18]. Last, whereas the zero-field signal indeed displays the gradual rise typically associated with defect-induced magnetism in correlated Fermi systems[19], the field-induced signal increases according to classical mean-field theory, suggesting a different and intrinsic mechanism (Fig. 3a).

Our data bear on two popular descriptions of copper oxide superconductors. The first states that the copper oxides are describable in the same terms as ordinary solids, where small variations of key parameters lead to Fermi-surface instabilities corresponding to superconductivity and insulating 'striped' phases. Within such an interpretation, stripe order is simply tuned by doping, and appears because of Fermi-surface nesting and lattice anomalies near $x = 1/8$. However, what we have found is that below $x = 1/8$, very modest (on the scale of both electron and phonon energies) fields induce antiferromagnetic order, with a field-independent onset temperature and a strongly field-dependent amplitude. These results cannot

follow from a simple Fermi 'quasiparticle' description, which anticipates that the Néel temperature will rise significantly as the base-temperature ordered moment increases.

A second description of high-T_c superconductivity does not focus on microscopic detail (unlike the quasiparticle-based theories), but is instead based on the hypothesis that the copper oxides possess hidden 'SO(5)' symmetry where magnetic and superconducting order parameters can be 'rotated' into each other. Calculations based on this hypothesis predict antiferromagnetic vortices in a magnetic field, and have had some success in modelling the data[20–23]. The original work was performed assuming that the symmetry is exact[20]. In this model the antiferromagnetism is confined to the vortex cores which have size $\sim\xi = 20$ Å, and there are no regions of the compound where superconductivity and antiferromagnetism exist simultaneously. Our data suggest that the antiferromagnetic regions are much bigger than this ($\zeta > 400$ Å), and extend well beyond the vortex cores into the superconducting areas. Alternatively, there could be interactions between the vortices that lead to coherent long-range antiferromagnetic order without the magnetism spreading beyond the cores; but then the corresponding Néel temperature would be a strong function of the intervortex spacing, controlled by H—whereas the onset temperature in our experiments is approximately field-independent.

More recent computations motivated by our experiments have relaxed SO(5) symmetry to allow coexistence of superconductivity and magnetism, with the antiferromagnetic correlations extending beyond the vortex cores into the bulk of the crystal[22,23]. Although the underlying continuum approximations may be called into question at high fields, such a model[23] gives quantitative results in good agreement with our data for $T = 0$, as shown in Fig. 3b. The physical insight here is that the magnetism of the vortex state manifests a magnetic quantum critical point very close to the superconductor in the phase diagram[24].

We now consider how our results relate to the wider understanding of high-T_c superconductivity. First, they provide clear evidence for intrinsic antiferromagnetism coexisting with superconductivity in the same sample. Because the relative amplitudes of the two types of order can be continuously tuned by a magnetic field using a fixed sample (rather than by changing the doping), experiments to examine the trade-offs between magnetism and superconductivity should become much more detailed and reliable. Second, our data taken together with resistivity measurements[25] strongly suggest that in a magnetic field large enough to destroy superconductivity ($H > H_{c2}$), an underdoped copper oxide would become an incommensurate, antiferromagnetic insulator. This means that if we want to construct a theory of superconductivity at $T = 0$ in underdoped copper oxides, the most obvious starting point is this antiferromagnetic insulator, and not—as in conventional theories based on a Bardeen–Cooper–Schrieffer approach—a metallic Fermi liquid of weakly interacting quasiparticles. □

Received 15 February; accepted 20 November 2001.

1. Monthoux, P., Balatsky, A. V. & Pines, D. Weak-coupling theory of high-temperature superconductivity in the antiferromagnetically correlated copper oxides. *Phys. Rev. B* **46,** 14803–14817 (1992).
2. Zaanen, J. & Gunnarson, O. Charged magnetic domain lines and the magnetism of high-T_c oxides. *Phys. Rev. B* **40,** 7391–7394 (1989).
3. Tranquada, J. M. *et al.* Evidence for stripe correlations of spins and holes in copper-oxide superconductors. *Nature* **375,** 561–563 (1995).
4. Kivelson, S. A., Fradkin, E. & Emery, V. J. Electronic liquid-crystal phases of a doped Mott insulator. *Nature* **393,** 550–553 (1998).
5. Zaanen, J. Stripes defeat the Fermi liquid. *Nature* **404,** 714–715 (2000).
6. Zaanen, J., Osman, O. Y. & van Saarloos, W. Metallic stripes: separation of spin, charge, and string fluctuation. *Phys. Rev. B* **58,** R11868–R11871 (1998).
7. Kittel, C. *Introduction to Solid State Physics* 6th edn, 317–358 (Wiley & Sons, New York, 1986).
8. Vaknin, D. *et al.* Antiferromagnetism in La_2CuO_4. *Phys. Rev. Lett.* **58,** 2802–2805 (1987).
9. Lee, Y. S. *et al.* Neutron-scattering study of spin-density wave order in the superconducting state of excess-oxygen-doped La_2CuO_{4+y}. *Phys. Rev. B* **60,** 3643–3654 (1999).
10. Kimura, H. *et al.* Neutron-scattering study of static antiferromagnetic correlations in $La_{2-x}Sr_xCu_{1-y}Zn_yO_4$. *Phys. Rev. B* **59,** 6517–6523 (1999).
11. Andoh, Y. *et al.* Resistive upper critical fields and irreversibility lines of optimally doped high-T_c cuprates. *Phys. Rev. B* **60,** 12475–12479 (1999).
12. Lake, B. *et al.* Spin gap and magnetic coherence in a clean high-temperature superconductor. *Nature* **400,** 43–46 (1999).
13. Wakimoto, S., Birgeneau, R. J., Lee, Y. S. & Shirane, G. Hole concentration dependence of the magnetic moment in superconducting and insulating $La_{2-x}Sr_xCuO_4$. *Phys. Rev. B* **63,** 172501–172505 (2001).
14. Katano, S., Sato, M., Yamada, K., Suzuki, T. & Fukase, T. Enhancement of static antiferromagnetic correlations by magnetic field in a superconductor $La_{2-x}Sr_xCuO_4$ with $x = 0.12$. *Phys. Rev. B* **62,** R14677–R14680 (2000).
15. Lake, B. *et al.* Spins in the vortices of a high temperature superconductor. *Science* **291,** 832–834 (2001).
16. Nohara, M. *et al.* Quasiparticle density of states of clean and dirty *d*-wave superconductors: mixed-state specific heat of $La_{2-x}Sr_xCuO_4$. *J. Phys. Soc. Jpn* **69,** 1602–1605 (2001).
17. Lake, B. *et al.* Antiferromagnetic vortex state in a high-temperature superconductor. Preprint cond-mat/0104026 at ⟨http://xxx.lanl.gov⟩ (2001).
18. Savici, A. T. *et al.* Static magnetism in superconducting stage-4 La_2CuO_{4+y} ($y = 0.12$). *Physica B* **289–290,** 338–342 (2000).
19. Aeppli, G. *et al.* Magnetic order and fluctuations in superconducting UPt_3. *Phys. Rev. Lett.* **60,** 615–618 (1988).
20. Arovas, D. P., Berlinsky, A. J., Kallin, C. & Zhang, S.-C. Superconducting vortex with antiferromagnetic core. *Phys. Rev. Lett.* **79,** 2871–2874 (1997).
21. Hedegård, P. Magnetic vortices in high-temperature superconductors. Preprint cond-mat/0102070 at ⟨http://xxx.lanl.gov⟩ (2001).
22. Hu, J.-P. & Zhang, S.-C. Theory of static and dynamic antiferromagnetic vortices in LSCO superconductor. Preprint cond-mat/0108273 at ⟨http://xxx.lanl.gov⟩ (2001).
23. Demler, E., Sachdev, S. & Zhang, Y. Spin ordering quantum transitions of superconductors in a magnetic field. *Phys. Rev. Lett.* **87,** 067202–067205 (2001).
24. Aeppli, G. *et al.* Nearly singular magnetic fluctuations in the normal state of a high-T_c superconductor. *Science* **278,** 432–435 (1997).
25. Boebinger, G. S. *et al.* Insulator-to-metal crossover in the normal state of $La_{2-x}Sr_xCuO_4$ near optimal doping. *Phys. Rev. Lett.* **77,** 5417–5420 (1996).
26. Kittel, C. *Introduction to Solid State Physics* 6th edn, 426–428 (Wiley & Sons, New York, 1986).

Acknowledgements

We thank P. Dai, P. Hedegård, S. Kivelson, H. Mook, J. Zaanen, S. Sachdev and S.-C. Zhang for discussions. Oak Ridge National Laboratory is managed by UT-Battelle, LLC, for the US Department of Energy. H.M.R. holds a Marie Curie fellowship funded by the European Community.

Correspondence and requests for materials should be addressed to B.L. (e-mail: bella.lake@physics.ox.ac.uk).

Shear instabilities in granular flows

David J. Goldfarb*†, Benjamin J. Glasser* & Troy Shinbrot*

** Department of Chemical and Biochemical Engineering, Rutgers University, Piscataway, New Jersey 08854-8058, USA*

Unstable waves have been long studied in fluid shear layers[1–3]. These waves affect transport in the atmosphere and oceans, in addition to slipstream stability behind ships, aeroplanes and heat-transfer devices. Corresponding instabilities in granular flows have not been previously documented[4], despite the importance of these flows in geophysical and industrial systems[5–7]. Here we report that breaking waves can form at the interface between two streams of identical grains flowing on an inclined plane downstream of a splitter plate. Changes in either the shear rate or the angle of incline cause such waves to appear abruptly. We analyse a granular flow model that agrees qualitatively with our experimental data; the model suggests that the waves result from competition between shear and extensional strains in the flowing granular bed. We propose a dimensionless shear number that governs the transition between steady and wavy flows.

Shear transmission in granular flow is intrinsic to systems ranging from geophysical flows to industrial processing, and peculiarities in granular shear response have consequences that can be dramatic or commonplace. More spectacular examples include

† Present address: Schering-Plough Research Institute, Kenilworth, New Jersey 07033, USA.